Desalination and Water Treatment
www.deswater.com

doi: 10.5004/dwt.2022.28847

272 (2022) 277–289
October

Effective adsorption and removal of industrial dye from aqueous solution using mesoporous zinc oxide nanoparticles via metal organic frame work: equilibrium, kinetics and thermodynamic studies

Ghaferah H. Al-Hazmi[a], Moamen S. Refat[b], Mohamed G. El-Desouky[c,*], Ashraf A. El-Bindary[d]

[a]*Department of Chemistry, College of Science, Princess Nourah bint Abdulrahman University, P.O. Box: 84428, Riyadh 11671, Saudi Arabia, email: ghalhazimi@pnu.edu.sa/dr.ghaferah@yahoo.com*
[b]*Department of Chemistry, College of Science, Taif University, P.O. Box: 11099, Taif 21944, Saudi Arabia, email: moamen@tu.edu.sa*
[c]*Egyptian Propylene and Polypropylene Company, Port Said 42511, Egypt, email: ch.moh.gamal@gmail.com*
[d]*Chemistry Department, Faculty of Science, Damietta University, Damietta 34517, Egypt, email: abindary@yahoo.com*

Received 13 June 2022; Accepted 18 August 2022

ABSTRACT

Pollution industrial dyes is a serious environmental issue and successful purifying has thus far proven to be a difficult task. Therefore, in study, environmentally safe zinc oxide nanoparticles were synthesized through calcination of zeolitic imidazolate framework 7 at various temperatures for calcination 450°C, 550°C and 650°C. The elimination of Congo red (CR) in wastewater samples was tested with good adsorption capability. Adsorption of CR using ZnO from aqueous solution. Scanning electron microscopy, Fourier-transform infrared spectroscopy, X-ray diffraction and the surface area and pore volume of ZnO were discovered during Brunauer–Emmett–Teller testing at 77 K to be 119.12 $m^2 \cdot g^{-1}$ and the total pore volume was 0.362 $cm^3 \cdot g^{-1}$. Adsorption at pH 3 was found the best for CR. Initial concentration and dosage, resulting in microporous surfaces that have a high potential to interact with and absorb CR. Adsorption tests demonstrated that ZnO had a good capability for removing CR (975 $mg \cdot g^{-1}$). However, after numerous reuse cycles, this performance was remained. The findings of the adsorption experiments demonstrated that the Langmuir equation for the adsorption isotherm and the pseudo-second-order model of the adsorption kinetics were compatible. Adsorption's activation energy was also found to be 24.7 $kJ \cdot mol^{-1}$, demonstrating that chemisorption process. The adsorption process was calculated, and it was shown to be both endothermic and spontaneous also determine thermodynamic parameter $\Delta G°$, $\Delta H°$ and $\Delta S°$. The mesoporous ZnO adsorbent proved to be a simple and effective water purification. ZnO material has shown promise in the process of removing CR from aqueous solution.

Keywords: Zinc oxide nanospheres; Adsorption isotherm; Thermodynamic parameters; Adsorption kinetics

1. Introduction

Several of the biggest and most important sectors on the earth is the colouring sector. However, due to the range of colors found in its effluent, it is considered a severe source of pollution for species in the environment. Some dyes have been shown to be genotoxic [1]. A few of the impacts of dyes on humans include kidney, liver, brain, reproductive system, and nervous system malfunction [2]. As a result, removal rate from the environment is a

* Corresponding author.

critical factor. Researchers are searching for inexpensive ways to remove these colours from the water. It is estimated that each year, 100 tons of dyes and pigments are released into waters by the textile industry [3]. To clean up wastewater or rivers of contaminants, a variety of approaches can be utilized. Biological, chemical, or physical purification techniques make up a majority of them [4]. Adsorption phenomena are the aggregation of adsorbates at the gas–solid or liquid–solid interface [5,6]. Adsorption is frequently reversible due to the obvious frequently van der Waals interactions between the adsorbent and the adsorbate [7]. Fundamental ideas in the study of adsorption technology include isotherm models. They discuss the interactions between adsorbent and adsorbate, and they can also be used to compute adsorption ability [7,8]. Chemical treatments, on the other hand, produce a terrible odor and waste and are expensive; adsorption phenomena are appealing for decolonization owing to its low cost, adaptable structure, and does not produce any harmful chemicals after removing the target substances. The biggest drawback of biological treatment techniques is how lengthy some of them can be. Mix bacterium decolorization, for example, can take up to 30 h to accomplish [9,10]. Some colors, contrasted with, are resistant to physical mechanism like ion exchange, and electro kinetic coagulation produces a large amount of sludge. Conversely, adsorption is economical, easy to use, and can eliminate almost all type of contaminants [11–13]. That's why this process is widely in use for removal of not only dyes and pigments, but also for other contaminants found in effluent or drainage, including such heavy metal pollutants [14].

Benjamin Feingold presented substantial evidence to the American Medical Association in 1973 regarding the connection between food additives and learning and behavior issues. That was nearly 45 y ago, that were subsequently associated with Attention Deficit Hyperactivity Disorder (ADHD). 1,200 people were used to study the efficacy of more than 3,000 different food additives, yet his research was not only refuted but also insulted. Over than 50% of the participants benefited, according to Feingold, from a diet free of these additives, which was also associated with a considerable reduction in hyperactive indicators [15,16]. Numerous investigations were conducted to determine the seriousness of this accusation, three of those were conducted at Southampton University and revealed the negative aspects of these dyes for the first time in a conclusive and scientific manner [17–19]. Within every trial, the use of a specific addition was stopped and then resumed while more than 100 kids from various age groups were observed for signs of irritability, restless, and sleep disturbance [20–22]. Impulsivity, a lack of patience, impulsivity, and inattentiveness are some of the signs of ADHD. Like hypertension, ADHD is a quantitative diagnosis, and some people who are on the edge of list includes may have their symptoms get worse even from a modest amount of these chemicals. Research suggests that edible dyes have a minor but negative impact on children's behavior that has not previously been associated with diagnosable ADHD. Food colorings therefore seem to be more of a public health issue than an ADHD issue [23].

Rivers are among the most significant landscape elements on the planet [24]. They transport surface nutrients and water to the seas through sediment regions. Rivers are important water sources as well as marine life, which provides food for humans and animals. Due to their importance in tourism and hydroelectricity production, rivers are a valuable resource in contemporary human society, and other activities. Regrettably, careless individuals and businesses also exploit waterways as dumping grounds for unwanted goods and chemicals [25]. The major threat to water security is believed to be direct dumping of contaminants without proper treatment, into water bodies from different sources. The textile coloring and processing sector, for example, is ranked as the tenth most major pollutants to rivers, contributing 17%–20% of all industrial water pollution1. About 5,000–10,000 synthetic dyes are discharged into the waterways each year as a result of their widespread use. Congo red (CR) has been one of the most popular dyes since their invention [26]. When dissolved in water, the molecules of this dye have negative charges, this accounts for the dyes' moniker of anionic dyes. Because when dye is accidentally spilled into surface waterways, prevents sunlight from penetrating the water (It is required for aquatic plant photosynthesis). It endangers the aquatic ecosystem as well as the people who live near the river. As a result, proper treatment of textile wastewater is critical for environmental and ecological protection [27,28]. Owing to its finite size, no crystal is flawless because it would expand in all directions to infinity. The diffraction peaks broaden as a result of the divergence from ideal crystallinity [29]. The two most important properties derived from peak width research are: (a) Dimensions of crystallites, and (b) strain in the lattice. Crystallite size serves as a proxy for coherent diffracting domain size. Since polycrystalline aggregates are present, the particle size and the crystallite size are not necessarily the same. Brunauer–Emmett–Teller (BET), light scattering, and Scanning and transmission electron microscopy are the two most often used techniques to measure particle size as opposed to crystallite size. The dispersion of lattice constants brought on by crystal imperfections including lattice dislocations is referred to as lattice strain [30]. One of the main sources of strain is the triple junction at the grain boundary. Other sources of strain include stacking faults, contact or sinter stresses, coherency stresses, and other strains. X-ray line broadening is used to examine the distribution of dislocations. In additional to alloying and reducing the size of the crystallites, the particles are under a great deal of extra pressure during mechanical alloying [31]. The use of X-ray characterization to determine a quick and efficient technique is to measure crystallite size and lattice strain [32,33].

Because of its high efficacy, ability to distinguish between a multitude of chemicals, a straightforward design, and viability from an economical perspective, adsorption on activated carbon is widely utilized [34]. Micropore volumes, extremely high surface areas, and excellent adsorption capacity, accelerated adsorption kinetics, generally simple renewal processes, and amphoteric characteristics, activated carbons are widespread to use as adsorbents in wastewater treatment. These characteristics allow for the adsorption

of both cationic and anionic contaminants in liquid waste. Despite this, the significant expense associated with using non-renewable and costly materials, such coal, means that the amount of based activated carbons is still restricted [35,36]. Activated carbons are currently somewhat expensive, but scientists are working to make them more affordable, more efficient, and environmentally benign. Lately, academics around the world have turned their attention to inexpensive precursors.

The goal of this work is reuse of zeolitic imidazolate framework 7 (ZIF-7) that is used for several times for adsorption we can used it again by different way through calcination it at different temperature to form ZnO and investigate its ability for molecules of the anionic dye (CR) being adsorbed from a solution in water. Research on batch kinetic and equilibrium were conducted to look at adsorption. The kinetics, isotherms, and thermodynamics of CR adsorption on synthesized ZnO were thus thoroughly examined. The influence of pH and competition anions were also investigated, as well as the adsorption mechanism.

2. Materials and methods

2.1. Materials and instruments

The materials and instrument used for characterization was illustrated in detail at (Supporting information) [37].

2.2. Preparation of the adsorbent

ZIF-7 was synthesized using the conventional hydrothermal synthetic method outlined previously, 1.19 g zinc nitrate hexahydrate and 0.473 g benzimidazole were dissolved in 90 mL N,N-dimethylformamide (DMF). Second, this reaction mixture was sealed in a 150 mL Teflon autoclave and heated at 140°C for 24 h (5°C/min heating rate). To get rid of DMF and other undissolved compounds, the hydrothermal processing materials are soaked in methanol for 24 h at room temperature. White ZIF-7 crystals were dried for 24 h at room temperature after the methanol was decanted. As the last step in the ZIF-7 method, the crystals were then dried for an additional 24 h at 110°C [38]. ZnO was produced by calcining ZIF-7 at 450°C, 550°C, and 650°C for 2 h at a rate of 5°C/min.

2.3. Preparation of adsorbate

The stock solution of CR (2.5×10^{-3} mol·L^{-1}) was organized by adding double-distilled water to a volumetric flask along with the dissolving quantity of CR. The stock solution was diluted with double-distilled water to the necessary concentration to create the working solutions [39].

2.4. Batch adsorption study experimental design

The CR adsorption on ZnO was accomplished using the batch equilibrium approach. A pH meter was used to modify with the dose 0.02–0.1 g sample of (ZnO) with a 25 mL CR solution of 1.22×10^{-3} mol·L^{-1} at various pHs (1–12) attained for 90 min by injecting a small amount of HCl or NaOH solution (1 M). All adsorption processes used the optimum pH, which was defined. A number of time intervals were investigated to measured if adsorption equilibrium and maximum CR removal might be attained. The answer was filtered using a Whatman (number 40) filter paper to get rid of any organic or inorganic induces produced under acidic or basic conditions. Each solution's equilibrium concentration was measured at a wavelength of UV-maximum (λ_{max}) at 488 nm. Additionally, CR adsorption investigations were conducted using a water bath with a shaker to create isotherms at various temperatures (25°C–50°C). Calibration curves were developed to link concentrations to different absorbance readings. Following the validation of the calibration curves, the highest wavelengths that corresponded to the absorption maxima for the CR were determined [39–41].

3. Results and discussion

3.1. Characterization of ZnO

3.1.1. X-ray diffraction patterns

The synthesized ZIF-7 X-ray diffraction (XRD) pattern was compared with JCPDS card No. 06-062-1030 that approved that ZIF-7 was synthesized efficiently [42]. The wurtzite structure may be seen in the XRD pattern of ZnO powder after calcination of ZIF-7 (Fig. 1). There are no more diffraction peaks corresponding to Zn, Zn(OH_2), or other ZnO phases are noticed, suggesting that pure ZnO nanoparticles are naturally crystalline. The peaks are crisp and narrow, demonstrating the excellent calibre of the sample, with fine particle size and good crystallinity. Lattice parameters were estimated using XRD data (a = 3.2491 Å and c = 5.2063 Å) [40,43].

3.1.1.1. Crystallite size and strain determination

3.1.1.1.1. Scherrer method

The spreading of peaks demonstrates grain refinement additionally to the powder's significant strain. The instrumental broadening (β_{hkl}) was corrected, matching to each ZnO diffraction peak using Eqs. (1) and (2) [44]:

$$\beta_{hkl\circledcirc} = \left[\left(\beta_{hkl} \right)_e^2 - \beta_{instrumental}^2 \right]^{1/2} \quad (1)$$

The average nanocrystalline size was calculated using Debye–Scherrer's formula [Eq. (2)]:

$$D = \frac{K\lambda}{\beta\cos\theta} \quad (2)$$

The peaks are sharp and narrow at 2° 37, indicating that the sample is of the highest calibre possible, possessing high crystallinity and tiny particles 17.64, 29.32 and 33.53 nm for calcinated ZnO at 450°C, 550°C and 650°C [45].

3.1.2. BET surface area

Fig. 3 depicts the ZnO's N_2 adsorption–desorption isotherm. The sample had a type II of pore model, indicating that microporosity and mesoporosity coexisted in ZnO

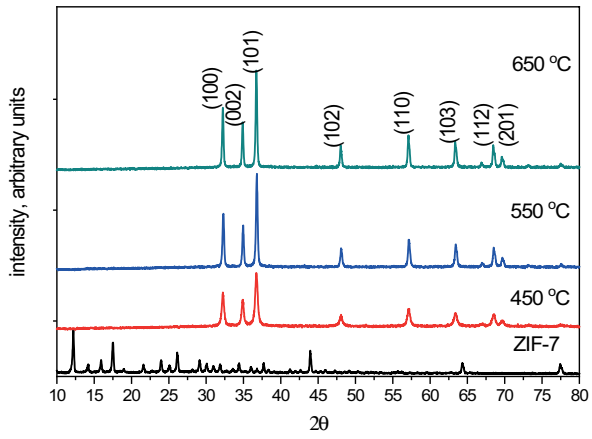

Fig. 1. Different calcination temperatures as seen in the XRD of ZIF-7 and ZnO (450°C, 550°C and 650°C).

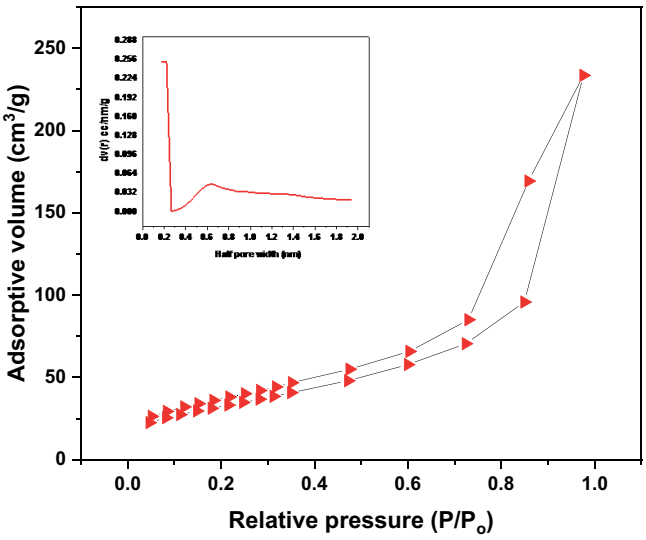

Fig. 2. N_2 sorption isotherm of ZnO.

at 450°C. The specific surface area (S_{BET}) was calculated to be around 119.12 m^2 g^{-1} and the total pore volume was 0.362 cm3·g^{-1}. It demonstrated that ZnO nanoparticles have a superior porosity morphology. According to the pore distribution Fig. 2, the average particle radius was calculated to be 1.16 nm. By using S_{BET} and potential active sites on the adsorbent, the CR adsorption was enhanced [46]. Additionally, the high pore size dispersion permitted quick CR molecule inter-diffusion across linked, low-resistance channels [47].

3.1.3. Scanning electron microscopy evaluation

Scanning electron microscopy (SEM) test was conducted to analyze the structural characteristics and morphology of ZnO. A SEM image of ZnO created by calcining ZIF-7 at 450°C is shown in Fig. 3. The average diameter of ZnO nanoparticles was roughly 20 nm, which was confirmed by SEM examination. So, as the calcination temperature increased, the ZnO grew longer [39,48].

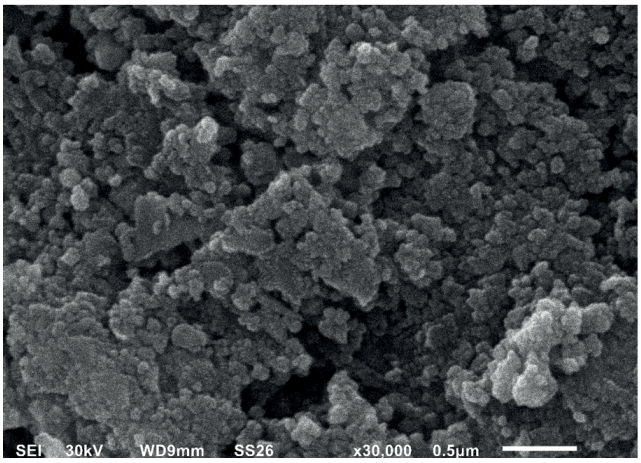

Fig. 3. ZnO in a SEM image at 450°C.

3.1.4. Determination of point of zero charge (pH_{PZC})

The results obtained pH_{PZC} value for ZnO at 450°C is shown in Fig. 4. The pH_{PZC} value of 5 for the ZnO at 450°C was determined. This result indicated that once the solution's pH is less than pH = 5. The ZnO surface possesses a positive charge that is conducive to anionic dye adsorption such as (CR), while above this value the surface charge is negative [39,49].

3.2. Batch experiments

3.2.1. Effect of pH

The adsorbent's surface charge and ionisation level are both influenced by the aqueous solution's pH. The importance of the liquid's pH as a key variable in the adsorption process when using stock concentration (1.22×10^{-3} mol·L^{-1}, 25°C and dosage 0.02 g/25 mL, contact time 60 min time) [50,51]. The effects of CR were studied and examined. Fig. 5 displays the influence of pH of initial solution on the adsorbed CR. As seen in Fig. 5, the adsorption optimum for ZnO was reported at pH 3, the largest quantity of adsorption was seen at pH 3, and the adsorption efficiency was enhanced. As can be shown, the CR adsorption increases as the pH drops under 5, this can result from the created functional group borders and the surface charge shift. Regarding the adsorption efficiency of CR was reduced when pH above 3, so can be concluded that at pH 3 the CR has maximum adsorption as well as strongly reacted with the ZnO [52,53].

3.2.2. Effect of calcination temperature

By means of ZnO at various calcination temperatures, the effect of ZnO (adsorbent) calcination temperature on CR sorption process was examined 450°C, 550°C, and 650°C [54–56]. The ZnO dosage was 0.02 g; the dye solution volume was 25 mL, the concentration was 1.22×10^{-3} mol·L^{-1}, the pH was 3, and the shaking speed was 200 rpm. The efficiency of adsorption of CR decreased from 99.8% > 83.79% > 82.23% by using ZnO at 450°C, 550°C

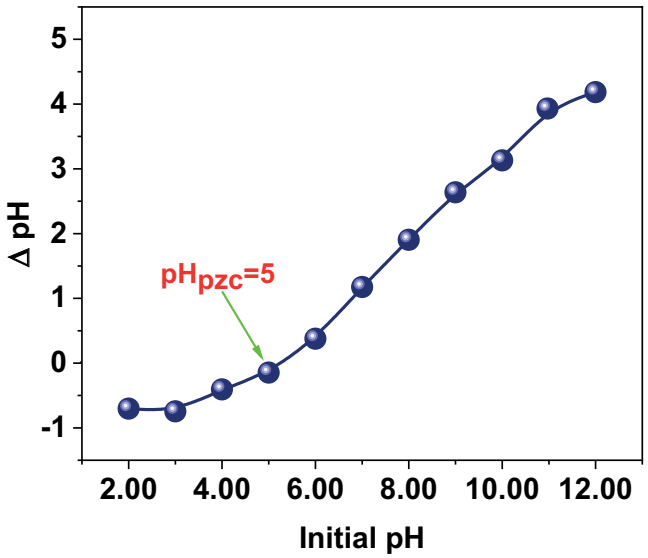

Fig. 4. pH_{PZC} of ZnO at the calcination temperature of 450°C.

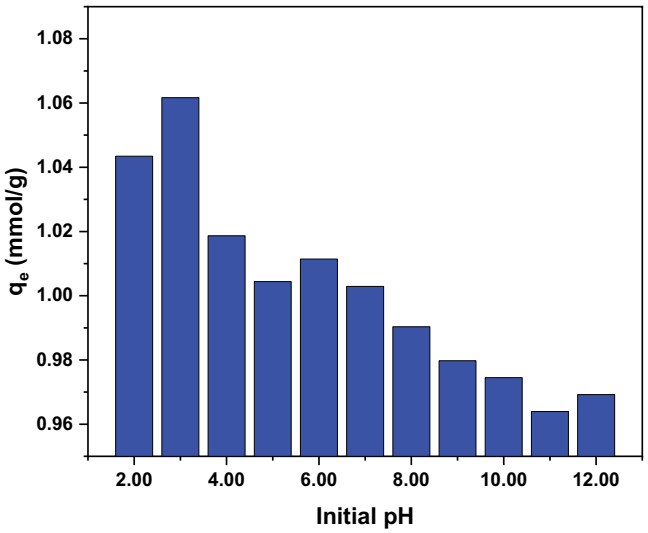

Fig. 5. pH impact on CR adsorption using ZnO as the adsorbent at 450°C.

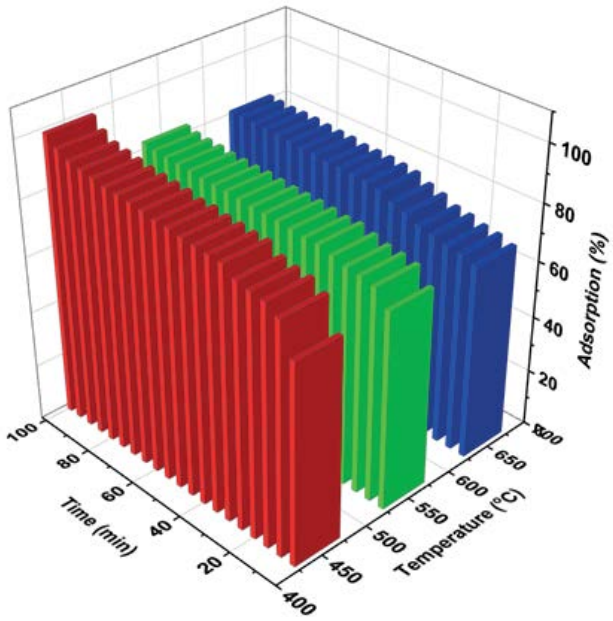

Fig. 6. Temperature-related effects on CR adsorption during calcination.

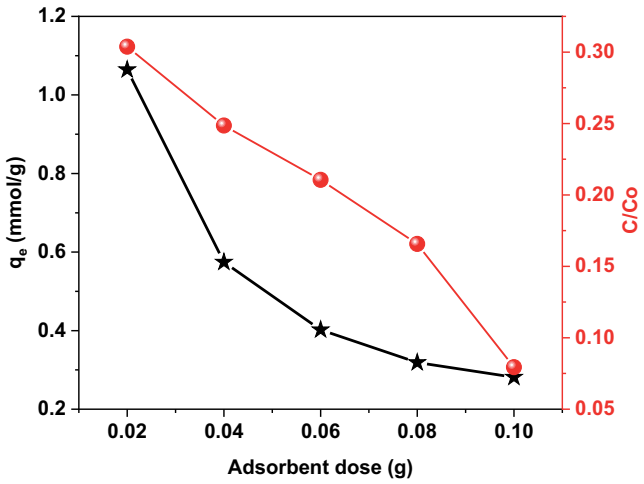

Fig. 7. CR adsorption and the dose of ZnO.

and 650°C, respectively as increasing in the particle size as the temperature of calcination increased (Fig. 6). As a result, At 450°C, higher CR adsorption onto decreased ZnO adsorbent particle size was responsible for the increased surface area's increased surface area's better accessibility of binding sites for bulk adsorption of the dye [40,57].

3.2.3. Effect of dose

Fig. 7 displays the result of different ZnO doses of 0.01–0.1 g per 25 mL on the CR concentration of 1.2×10^{-3} mol·L^{-1} at 25°C and pH 3. As the ZnO dose was raised from 0.01 to 0.1 g, the percentage of ZnO removed rose. This increase is the result of increased surface area, which increases the unoccupied site for a fixed number of CR molecules up to a specific limit. As the adsorbent surface area expands and the dose rises, the equilibrium concentration of (CR) drops [58].

3.2.4. Adsorption isotherm

The adsorption analysis was done in the current research in relation to the Freundlich [59], Langmuir [60,61], Temkin [62], and Dubinin–Radushkevich [63] isotherm models. These models were applied to improve the layout of an adsorption process for the CR adsorption at ZnO.

According to the Langmuir isotherm, the identical and homogeneous adsorption energies exist at every adsorption site on the surface of the adsorbent. A monolayer of adsorbed molecules covers the adsorbent surface and there is no contact between the adsorbed molecules on the

ZnO surface Fig. 9. The Langmuir adsorption isotherm can be given by Eq. (3):

$$\frac{C_e}{q_e} = \frac{1}{q_m K_L} + \frac{C_e}{q_m} \tag{3}$$

A model for explaining heterogeneous systems that is based on real data is the Freundlich isotherm Fig. 8. It suggests that the adsorbed molecules engage in interaction with the variable binding sites of the adsorbent; Eq. (4) lends support to this idea:

$$\ln q_e = \ln K_F + \frac{1}{n}\ln C_e \tag{4}$$

The Freundlich isotherm suggests that the heat of adsorption is logarithmic, however the Temkin model states that it is provided in equations. Fig. 8 Temkin model is signified as Eq. (5) [64]:

$$q_e = \beta_T \ln K_T + \beta_T \ln C_e \tag{5}$$

The Dubinin–Radushkevich isotherm is employed to measured the usual porosity and the perceived free energy of adsorption. It assists in distinguishing whether adsorption investigations are physical or chemical in origin. Eq. (6) gives the linear form:

$$\ln q_e = \ln Q_{DR} - K_{DR}\varepsilon^2 \tag{6}$$

With the value, this energy reveals whether the adsorption is chemical or physical of $8 < E < 16$ kJ·mol^{-1}, the chemical method is followed by the adsorption procedure, whereas the quantities are of $E < 8$ kJ·mol^{-1}. The adsorption mechanism is a physical one. The fact that the adsorption energy of CR at ZnO was 24.7 kJ·mol^{-1} demonstrates that chemisorption was the reaction (Table 1) [39,64].

3.2.5. Adsorption kinetics and mechanism studies

Pseudo-first-order kinetics can be used to explain the adsorption [65]. The experimental values have been fitted using the equations shown below.

$$\log\left(q_e - q_t\right) = \log q_e - \left(\frac{K_1}{2.303}\right)t \tag{7}$$

The pseudo-second-order model [66] can be utilized to convey the subsequent linear shape [Eq. (8)]:

$$\frac{t}{q_t} = \frac{1}{K_2 q_e^2} + \frac{t}{q_e} \tag{8}$$

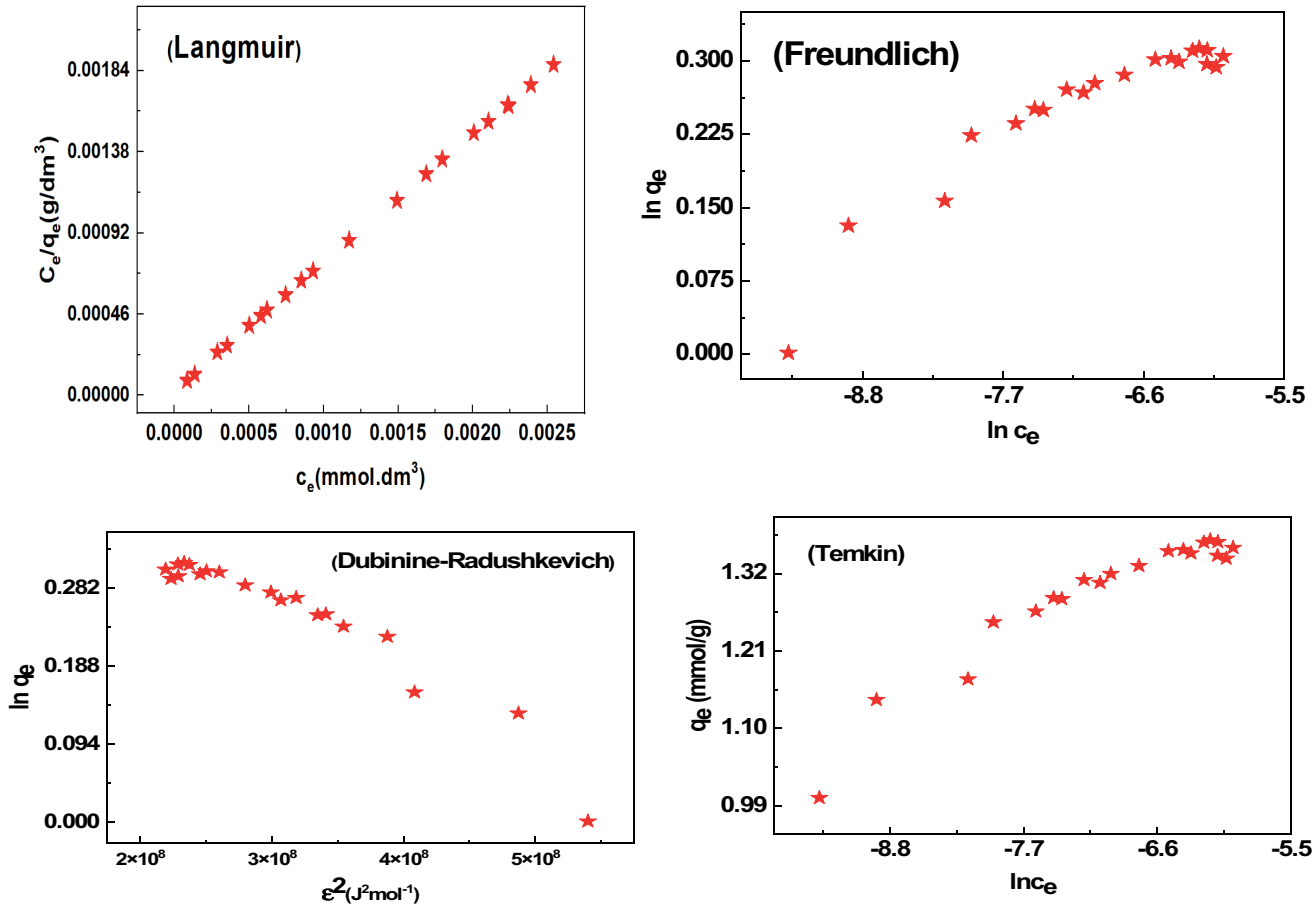

Fig. 8. ZnO isothermal sorption plots that are linearized.

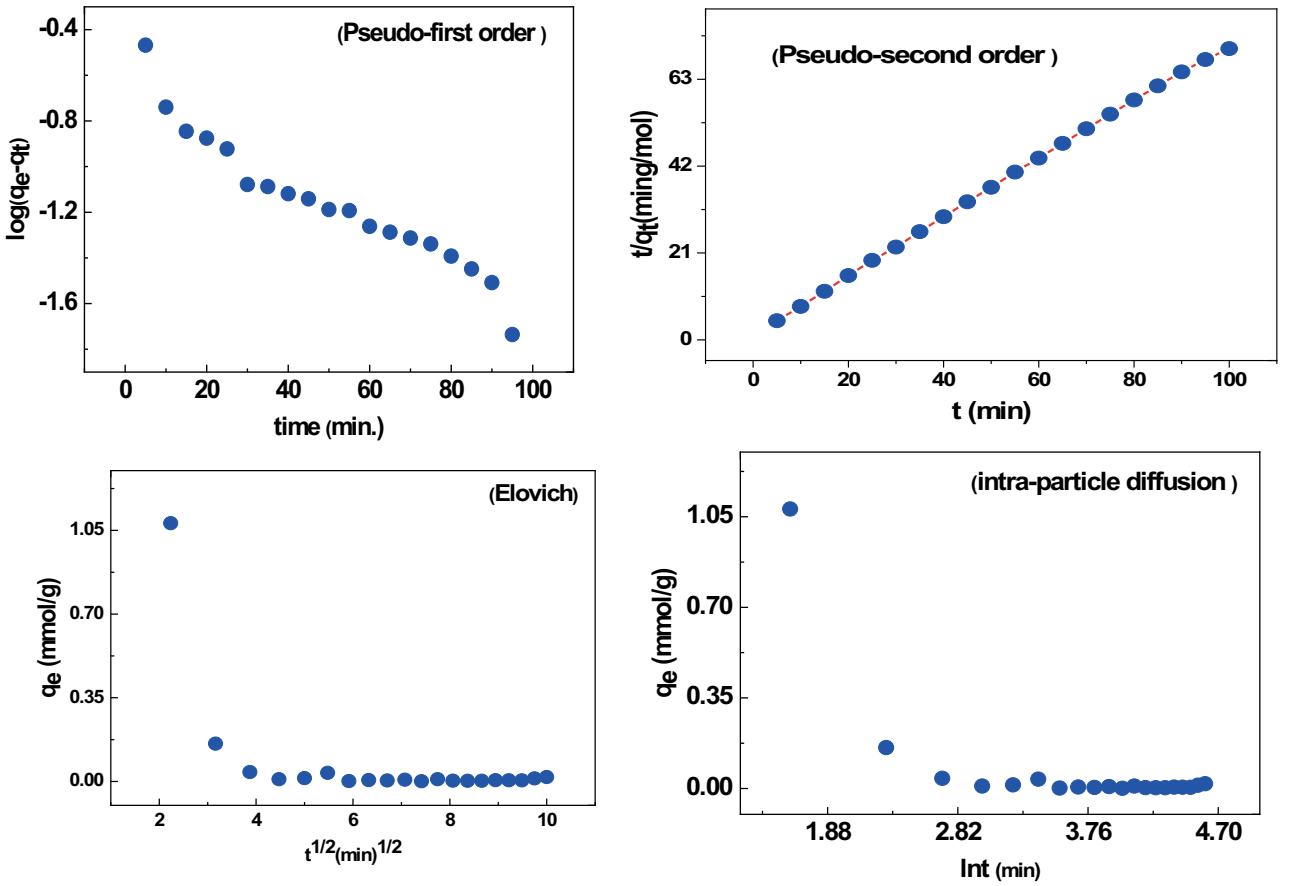

Fig. 9. Linearized adsorption kinetics of CR onto ZnO.

The Elovich model [67] can be used to illustrate the following Eq. (9):

$$q_t = \frac{1}{\beta}\ln(\alpha\beta) + \frac{1}{\beta}\ln t \tag{9}$$

The intraparticle diffusion model [66] is a well-liked technique to forecast the rate-controlling step. Eq. (10) is used to calculate the rate constants of intra-particle diffusion (K_i) at stage i.

$$q_t = K_i t^{1/2} + X \tag{10}$$

As seen in Fig. 10, the fitting straight lines were used to judge the accuracy of every kinetic model. The required kinetic models and computation coefficients are listed in Table 2. The estimates of the coefficient of determination (R^2 derived from the pseudo-first-order linear plot and Elovich (Fig. 9) models are very small (R^2 = 0.919 and 0.436) (Table 2). Hence, it is impossible to use these two models to the adsorption experiments of CR onto ZnO. The coefficient of determination is greater for the pseudo-second-order model (R^2 = 0.999) (Fig. 9), suggesting that the pseudo-second-order model well describes the experimental results and that adsorption is a chemical-controlling mechanism. The adsorption mechanism might be adequately explained by the intra-particle diffusion concept. The graphs of q_t vs. $t^{1/2}$ in Fig. 9 reveal multi-linearity characterizations, implying that more than one diffusion step occurs. The first section avoids going through the origin by being more angular. It implies that not only is intra-particle diffusion

Table 1
CR adsorption isotherms and their linear forms on ZnO nanoparticles

Isotherm	Value of parameters	
Langmuir	$q_{m,exp}$ (mmol·g^{-1})	1.3675
	q_m (mmol·g^{-1})	1.3811
	K_L (L·mmol^{-1})	248,387.968
	R^2	0.9999
Freundlich	n	13.56852
	K_F (mmol·g^{-1})(L·mmol^{-1})$^{1/n}$	0.77284
	R^2	0.86585
Dubinin–Radushkevich	q_{DR}	0.50744
	K_{DR} (J^2·mol^{-2})	–8.18E-10
	E_a (kJ·mol^{-1})	24.7
	R^2	0.903
Temkin	b_T (L·mol^{-1})	27,670
	A_T (kJ·mol^{-1})	21.47
	R^2	0.8907

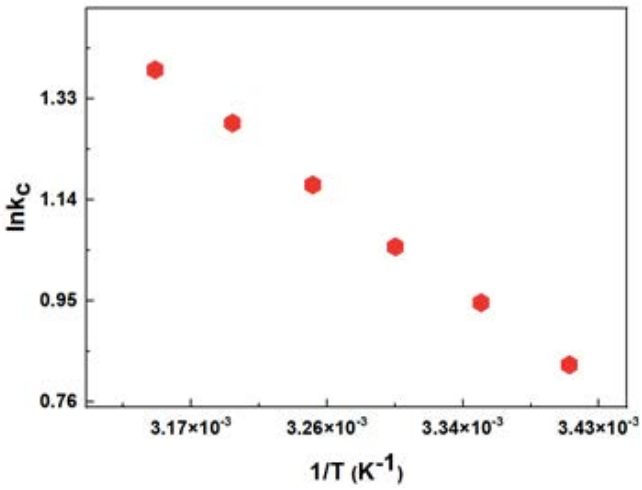

Fig. 10. For CR adsorption onto the ZnO adsorbent, van't Hoff plots are produced.

Table 2
Adsorption of CR onto ZnO nanoparticles was calculated using kinetic parameters and correlation coefficients

Model	Value of parameters	
Pseudo-first-order kinetic	K_1 (min^{-1})	0.64906
	q_e (mmol·g^{-1})	–0.01
	R^2	0.91946
Pseudo-second-order kinetic	K_2 (g·mg^{-1}·min^{-1})	0.3245
	q_e (mmol·g^{-1})	1.424
	R^2	0.99956
Intraparticle diffusion	K_i (mg·g^{-1}·min$^{1/2}$)	–0.0574
	X (mg·g^{-1})	0.46639
	R^2	0.25947
Elovich	β (g·mg^{-1})	–4.9596
	α (mg·g^{-1}·min^{-1})	2.28
	R^2	0.4365
Experimental data	$q_{e,exp}$ (mmol·g^{-1})	1.4

a rate-controlling step, but it is also influenced by the boundary layer diffusion process. The gradual adsorption stage is the second suppressed stage, when intra-particle diffusion slows down due to the incredibly low concentration of CR still present in the solution [69].

3.2.6. Thermodynamic modelling studies

The thermodynamic variables affecting the adsorption mechanism, ($\Delta H°$, kJ·mol^{-1}), ($\Delta S°$, J·mol^{-1}·K^{-1}) and ($\Delta G°$, kJ·mol^{-1}) may be assessed by Eqs. (11) and (12):

$$\Delta G° = -RT \ln K_c \tag{11}$$

$$\Delta G° = \Delta H° - T\Delta S° \tag{12}$$

Eqs. (13) can be expressed as Fig. 10:

$$\ln K_C = -\frac{\Delta H°}{RT} + \frac{\Delta S°}{R} \tag{13}$$

As soon as the temperature rose from 298 to 318 K, the negative ($\Delta G°$) results demonstrated the adsorption mechanism's viability and spontaneity (Table 3). Suggesting that adsorption was occurring more spontaneously, the amplitude of the free energy change rose to a negative value at elevated temperature estimates of the common enthalpy change that are positive ($\Delta H°$), which were 17.3 kJ·mol^{-1} for CR adsorption. The positive ($\Delta S°$) revealed an At the solid–liquid interface during the adsorption process, there is a rise in disorder or unpredictability, proving that the contact between the CR molecule and ZnO was endothermic in nature [68,69].

In this situation, CR of the zero standard free energy temperature ($T°$) is predicted to be 286 K. The low $T°$ values show that the investigated adsorbents are functional and can remove CR at very low temperatures.

3.2.7. Influence of electrolytes on the adsorption efficiency

The influence of ionic strength on ZnO efficiency against CR was thoroughly predicted in order to test ZnO's performance in actual treating wastewater. The quantity of additional rival (co-interfering) ions in the aqueous solution has a considerable impact on CR purification as seen in Fig. 11. Slight decrease in ZnO loading capacity, the competitor's density has increased (i.e., Cl^-), the adsorbent's adsorption capacities are still impressive of 1.62 mmol·g^{-1} (R% = 88.59%) for CR. The slightly noted discrepancy can be explained as follows from a broad perspective. The struggle between negatively charged anionic ions is intensifying (Cl^-) and CR molecules disturbed CR molecules interact with the ZnO adsorbent surface. Furthermore, increasing the concentration of electrolyte counter ions protected the ZnO surface and slowed the adsorption process. Additionally, as the salinity of the solution rose, the double electric layer shrank, creating an attractive force between the CR and the adsorbent surface. Other studies have found that inorganic competitors have antagonistic effects on CR adsorption using diverse adsorbents, which is a more honest description.

3.3. Comparison with other adsorbents

Inorganic mineral adsorbents, such as nanoparticles, nanocomposite, graphene-based materials, and others, have recently been created for the elimination of CR from wastewater by a lot of researches. A simple comparison (Table 4) reveals that the ZnO adsorbent has better CR adsorption capabilities than the other adsorbents.

3.4. Numeric adjustment

With the help of the two sophisticated models, all adsorption isotherms were corrected. Three error coefficients were determined through numerical simulation of the experimental isotherms:

Table 3
$\Delta G°$, $\Delta S°$, $\Delta H°$ during CR adsorption on ZnO

Dye	T (K)	$\Delta H°$ (kJ·mol^{-1})	$\Delta S°$ (J·mol^{-1}·K^{-1})	$T°$ (K)	$-\Delta G°$ (kJ·mol^{-1})
	298				1.72
	303				2.46
CR	308	17.3	65.9	262.49	3.21
	313				3.97
	318				4.7

Table 4
Highest CR dye adsorption capabilities of different adsorbents

Adsorbent	q_m (mg·g^{-1})	Reference
Dolomite	229.2	[70]
Banana peel powder	164.6	[71]
MoO_2/$CaSO_4$ composites	853.5	[72]
Hierarchical C/NiO-ZnO nanocomposite	613	[73]
Hydroxyapatite nanoparticles loaded on zein	416.7	[74]
Amine-modified *Funalia trogii* biomass	193.7	[75]
Pineapple plant stem	12	[76]
ZnO	975.38	This work

- As the R^2 value of the first correlation coefficient approaches one, it clearly shows how good the correction is.
- The second coefficient RMSE residual root mean square.
- AIC, the third error coefficient, is an effective metric for comparing the two models' corrections; the model that best fits the microscopic understanding of the test findings is the one with the lowest AIC score.

The following situations show that a recommended model fits the research observations well: R^2 tends to unity parameters should have values are within ±2 RMSE of their genuine values. Additionally, the AIC coefficient ought to be as small as possible.

Table 5 displays the R^2, RMSE, and AIC coefficients that were determined by modifying the observed isotherms to use the adsorption isotherm and kinetic models. In light of the constants each system needs, we make the following decision after the conclusion:

As a result of the error coefficients adhering to the eligibility criteria, For CR adsorption on ZnO, the Langmuir and pseudo-second-order models were determined to be suitable (R^2 is the highest, and RMSE and AIC are the least). Therefore, it is believed that electrostatic interactions between the positively charged ZnO surface and the negatively charged dye ion play a role in CR adsorption on ZnO.

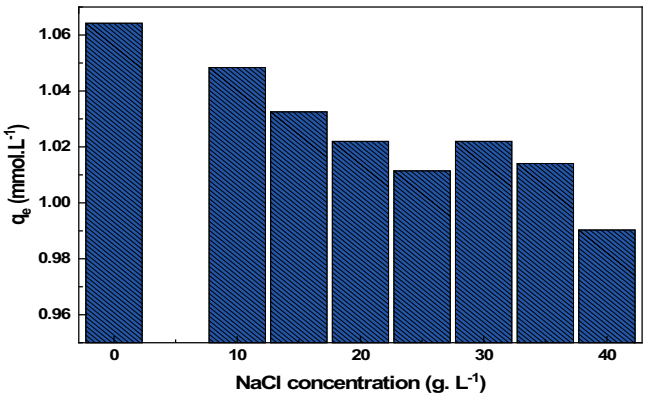

Fig. 11. Effect of NaCl on CR adsorption onto the ZnO at 450°C adsorbent (C_0: 1.22 × 10^{-3} mmol L^{-1}; initial pH 3; T: 25°C ± 1°C; sorbent dosage: 0.02 g/25 mL).

Table 5
R^2, RMSE (remaining root mean square error), and AIC (Akaike Information Criterion) values

Adsorption model	R^2	RMSE	AIC
Langmuir	0.9999	0.76	8.6
Pseudo-second-order	0.9995	0.84	7.4

3.5. Recycling of ZnO adsorbent

The value of adsorbent renewal in practical applications cannot be overstated. By placing 0.02 g of the adsorbent ZnO in the bottle and thoroughly washing many times with 0.01 M HCl until pH was 7, adsorption experiments of the CR from the ZnO were carried out, Unlike varied results described in the literature, rinse multiple times with distilled water first. The leftover CR was then eliminated using ethanol, and the residual adsorbent was recovered and heated to 60°C for 4 h. After regeneration, the adsorbent is prepared for the next phase of absorption. For CR, the regeneration efficiency was found to be

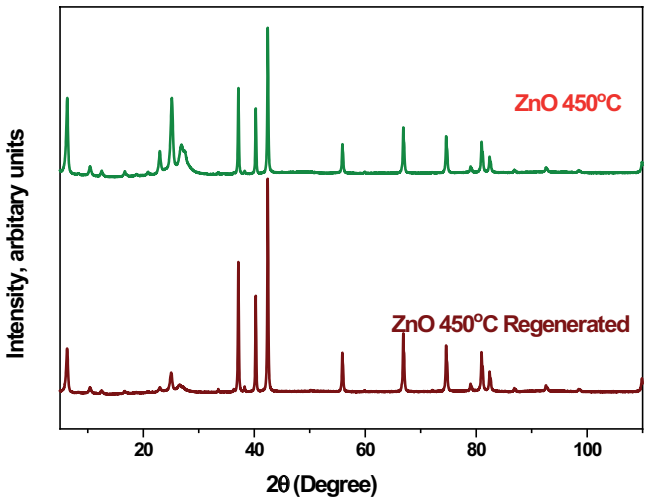

Fig. 12. XRD spectrum of ZnO 450°C and ZnO 450°C regenerated.

97.6%, 92.5%, and 88.6% for each adsorption/desorption cycle individually. This might be caused by restricted ZnO adsorption sites. We used XRD to analyse the ZnO material after testing and evaluation cycles and found that the crystallinity and structure were still there (Fig. 12). According to this research, ZnO has a good recyclability characteristic.

4. Conclusions

An effective ZnO for removing anionic dyes from the water was created in this research. At 298 K, the highest adsorption efficiency of reactive dyes CR was founded to be 1.4 mmol·g^{-1}. Langmuir was discovered to be a superior fit for this adsorption mechanism. Studies into thermodynamics showed that dye adsorption is more advantageous at higher temperatures; the positive value of enthalpy for CR adsorption implies an endothermic process, implying that the mechanism is Chemisorption. The kinetic models' usefulness for dye adsorption on ZnO was also examined. The dye's adsorption kinetics were pseudo-second-order. The process governing the adsorption of CR onto ZnO was pH-dependent, with the most efficient removal occurring at pH 3. The addition of electrolytes NaCl reduced the adsorption capacity of CR. The efficacy of the adsorbent to extract CR will decrease if the dye solution contains a larger concentration or more valences of other NaCl. The Scherrer formula, contrasted with, broadens the peak line from XRD pattern broadening of ZnO nanoparticles owing to finite crystallite size, the surface area was found 119.12 m^2·g^{-1} and pore size determined was 0.362 cm^3·g^{-1}. The effect of temperature was found to be endothermic and spontaneous.

Acknowledgements

Princess Nourah bint Abdulrahman University Researchers Supporting Project number (PNURSP2022R76), Princess Nourah bint Abdulrahman University, Riyadh, Saudi Arabia.

Symbols

q_e	—	Adsorbed amount of dye at equilibrium concentration, mmol·g^{-1}
q_{mL}	—	Maximum sorption capacity (corresponding to the saturation of the monolayer, mmol·g^{-1})
K_L	—	Langmuir binding constant which is related to the energy of sorption, L·mmol^{-1}
C_e	—	Equilibrium concentration of dyes in solution
K_F	—	Freundlich constants related to the sorption capacity, mmol·g^{-1}, (L·mmol^{-1})$^{1/n}$
n	—	Intensity
K_{DR}	—	Constant related to the sorption energy, J^2·mol^{-2}
q_{DR}	—	Theoretical saturation capacity, mmol·g^{-1}
ε	—	Polanyi potential, J^2·mol^{-2}
R	—	Gas constant, 8.314 J·mol^{-1}·K^{-1}
T	—	Temperature where the adsorption occurs
A_T	—	Temkin isotherm constant
b_T	—	Temkin constant in relation to heat of adsorption, J·mol^{-1}
q_t	—	Amount of dye adsorbed, mmol·g^{-1}
K_1	—	Rate constant for pseudo-first-order constant for the adsorption processes, min^{-1}
q_2	—	Maximum adsorption capacity for pseudo-second-order
K_2	—	Rate constant for pseudo-first-order constant for the adsorption processes, g·mg^{-1}·min^{-1}
α	—	Chemical adsorption rate, mg·g^{-1}·min^{-1}
β	—	Coefficient in relation with extension of covered surface
$\Delta G°$	—	Free Gibb's energy
$\Delta H°$	—	Enthalpy
$\Delta S°$	—	Entropy
K_c	—	distribution coefficient
C_{eq}	—	Concentration at equilibrium, mg·L^{-1}

References

[1] R. Bhattacharyya, S.K. Ray, Removal of Congo red and methyl violet from water using nano clay filled composite hydrogels of poly acrylic acid and polyethylene glycol, Chem. Eng. J., 260 (2015) 269–283.
[2] V. Vimonses, B. Jin, C.W.K. Chow, Insight into removal kinetic and mechanisms of anionic dye by calcined clay materials and lime, J. Hazard. Mater., 177 (2010) 420–427.
[3] R. Han, D. Ding, Y. Xu, W. Zou, Y. Wang, Y. Li, L. Zou, Use of rice husk for the adsorption of Congo red from aqueous solution in column mode, Bioresour. Technol., 99 (2008) 2938–2946.
[4] H. Zhu, R. Jiang, L. Xiao, Y. Chang, Y. Guan, X. Li, G. Zeng, Photocatalytic decolorization and degradation of Congo red on innovative crosslinked chitosan/nano-CdS composite catalyst under visible light irradiation, J. Hazard. Mater., 169 (2009) 933–940.
[5] M. Bhaumik, R. McCrindle, A. Maity, Efficient removal of Congo red from aqueous solutions by adsorption onto interconnected polypyrrole–polyaniline nanofibres, Chem. Eng. J., 228 (2013) 506–515.
[6] N. Hassan, A.Z. El-Sonbati, M.G. El-Desouky, Synthesis, characterization, molecular docking and DNA binding studies of Cu(II), Ni(II), Zn(II) and Mn(II) complexes, J. Mol. Liq., 242 (2017) 293–307.
[7] G. Vijayaraghavan, S. Shanthakumar, Performance study on algal alginate as natural coagulant for the removal of Congo red dye, Desal. Water Treat., 57 (2016) 6384–6392.
[8] M.G. El-Desouky, M. Abd El-Wahab, A.A. El-Bindary, Interpretations and DFT calculations for polypropylene/cupper

oxide nanosphere, Biointerface Res. Appl. Chem., 12 (2021) 1134–1147.
[9] M. Teotia, A. Mittal, R.K. Soni, Chapter 3 – Light-Mediated Thermoset Polymers, V. Grumezescu, A.M. Grumezescu, Eds., Materials for Biomedical Engineering: Thermoset and Thermoplastic Polymers, Elsevier, 2019, pp. 57–103.
[10] J. Mittal, Recent progress in the synthesis of layered double hydroxides and their application for the adsorptive removal of dyes: a review, J. Environ. Manage., 295 (2021) 113017, doi: 10.1016/j.jenvman.2021.113017.
[11] A. Mittal, J. Mittal, Chapter 11 – Hen Feather: A Remarkable Adsorbent for Dye Removal, S.K. Sharma, Ed., Green Chemistry for Dyes Removal from Wastewater: Research Trends and Applications, Scrivener Publishing LLC, USA, 2015, pp. 409–457.
[12] C. Arora, S. Sonia, P. Bajpai, J. Mittal, A. Mariyam, Chapter 14 – Dye Removal from Waste Water Using Metal Organic Frameworks, P. Singh, C.M. Hussain, S. Rajkhowa, Eds., Management of Contaminants of Emerging Concern (CEC) in Environment, 2021, pp. 375–394.
[13] A. Mariyam, J. Mittal, F. Sakina, R.T. Baker, A.K. Sharma, A. Mittal, Efficient batch and fixed-bed sequestration of a basic dye using a novel variant of ordered mesoporous carbon as adsorbent, Arabian J. Chem., 14 (2021) 103186, doi: 10.1016/j.arabjc.2021.103186.
[14] N. Hassan, A. Shahat, A. El-Didamony, M.G. El-Desouky, A.A. El-Bindary, Synthesis and characterization of ZnO nanoparticles via zeolitic imidazolate framework-8 and its application for removal of dyes, J. Mol. Struct., 1210 (2020) 128029, doi: 10.1016/j.molstruc.2020.128029.
[15] J. Mittal, P. Ahmad, A. Mittal, Kahwa tea (*Camellia sinensis*) carbon — a novel and green low-cost adsorbent for the sequestration of titan yellow dye from its aqueous solutions, Desal. Water Treat., 227 (2021) 404–411.
[16] A. Patel, S. Soni, J. Mittal, A. Mittal, C. Arora, Sequestration of crystal violet from aqueous solution using ash of black turmeric rhizome, Desal. Water Treat., 220 (2021) 342–352.
[17] J. Mittal, R. Ahmad, A. Mariyam, V. Gupta, A. Mittal, Expeditious and enhanced sequestration of heavy metal ions from aqueous environment by papaya peel carbon: a green and low-cost adsorbent, Desal. Water Treat., 210 (2021) 365–376.
[18] C. Arora, P. Kumar, S. Soni, J. Mittal, A. Mittal, B.J.D. Singh, Efficient removal of malachite green dye from aqueous solution using *Curcuma caesia* based activated carbon, Desal. Water Treat., 195 (2020) 341–352.
[19] N. Ranga, E. Poonia, S. Jakhar, A.K. Sharma, A. Kumar, S. Devi, S. Duhan, Enhanced antimicrobial properties of bioactive glass using strontium and silver oxide nanocomposites, J. Asian Ceram. Soc., 7 (2019) 75–81.
[20] A.K. Sharma, Y. Sharma, p-toluene sulfonic acid doped polyaniline carbon nanotube composites: synthesis via different routes and modified properties, J. Electrochem. Sci. Eng., 3 (2013) 47–56, doi: 10.5599/jese.2013.0029.
[21] A.K. Sharma, I. Singh, A rapid spectrophotometric method for trace determination of zinc, Food Anal. Methods, 2 (2009) 311–316.
[22] V. Kumar, P. Saharan, A.K. Sharma, A. Umar, I. Kaushal, A. Mittal, Y. Al-Hadeethi, B. Rashad, Silver doped manganese oxide-carbon nanotube nanocomposite for enhanced dye-sequestration: isotherm studies and RSM modelling approach, Ceram. Int., 46 (2020) 10309–10319.
[23] J. Mittal, Permissible synthetic food dyes in India, Resonance, 25 (2020) 567–577.
[24] V. Vimonses, S. Lei, B. Jin, C.W.K. Chow, C. Saint, Kinetic study and equilibrium isotherm analysis of Congo red adsorption by clay materials, Chem. Eng. J., 148 (2009) 354–364.
[25] H.-Y. Zhu, Y.-Q. Fu, R. Jiang, J.-H. Jiang, L. Xiao, G.-M. Zeng, S.-L. Zhao, Y. Wang, Adsorption removal of Congo red onto magnetic cellulose/Fe_3O_4/activated carbon composite: equilibrium, kinetic and thermodynamic studies, Chem. Eng. J., 173 (2011) 494–502.
[26] S. Moradi, S. Dadfarnia, A. Haji Shabani, S. Emami, Removal of Congo red from aqueous solution by its sorption onto the metal organic framework MIL-100 (Fe): equilibrium, kinetic and thermodynamic studies, Desal. Water Treat., 56 (2015) 709–721.
[27] L. Wu, Y. Liu, L. Zhang, L. Zhao, A green-chemical synthetic route to fabricate a lamellar-structured $Co/Co(OH)_2$ nanocomposite exhibiting a high removal ability for organic dye, Dalton Trans., 43 (2014) 5393—5400.
[28] A.A. El-Bindary, M.G. El-Desouky, M.A.M. El-Afify, Thermal and spectroscopic studies of some prepared metal complexes and investigation of their potential anticancer and antiviral drug activity against SARS-CoV-2 by molecular docking simulation, Biointerface Res. Appl. Chem., 12 (2022) 1053–1075.
[29] I. Gul, A. Maqsood, M. Naeem, M.N. Ashiq, Optical, magnetic and electrical investigation of cobalt ferrite nanoparticles synthesized by co-precipitation route, J. Alloys Compd., 507 (2010) 201–206.
[30] H. Irfan, M. Racik K., S. Anand, Microstructural evaluation of $CoAl_2O_4$ nanoparticles by Williamson–Hall and size–strain plot methods, J. Asian Ceram. Soc., 6 (2018) 54–62.
[31] N. Ballarini, F. Cavani, S. Passeri, L. Pesaresi, A.F. Lee, K. Wilson, Phenol methylation over nanoparticulate $CoFe_2O_4$ inverse spinel catalysts: the effect of morphology on catalytic performance, Appl. Catal., A, 366 (2009) 184–192.
[32] M. Salavati-Niasari, F. Davar, Synthesis of copper and copper(I) oxide nanoparticles by thermal decomposition of a new precursor, Mater. Lett., 63 (2009) 441–443.
[33] T.A. Altalhi, M.M. Ibrahim, G.A. Mersal, M.H.H. Mahmoud, T. Kumeria, M.G. El-Desouky, A.A. El-Bindary, M.A. El-Bindary, Adsorption of doxorubicin hydrochloride onto thermally treated green adsorbent: equilibrium, kinetic and thermodynamic studies, J. Mol. Struct., 1263 (2022) 133160, doi: 10.1016/j.molstruc.2022.133160.
[34] L.S. Oliveira, A.S. Franca, T.M. Alves, S.D. Rocha, Evaluation of untreated coffee husks as potential biosorbents for treatment of dye contaminated waters, J. Hazard. Mater., 155 (2008) 507–512.
[35] T.M. Alslaibi, I. Abustan, M.A. Ahmad, A.A. Foul, Cadmium removal from aqueous solution using microwaved olive stone activated carbon, J. Environ. Chem. Eng., 1 (2013) 589–599.
[36] M.G. El-Desouky, A.A. El-Bindary, M.A.M. El-Afify, N. Hassan, Synthesis, characterization, theoretical calculation, DNA binding, molecular docking, anticovid-19 and anticancer chelation studies of some transition metal complexes, Inorg. Nano-Metal Chem., 52 (2022) 1273–1288.
[37] M.A. El-Bindary, M.G. El-Desouky, A.A. El-Bindary, Metal–organic frameworks encapsulated with an anticancer compound as drug delivery system: synthesis, characterization, antioxidant, anticancer, antibacterial, and molecular docking investigation, Appl. Organomet. Chem., 36 (2022) e6660, doi: 10.1002/aoc.6660.
[38] H.A. Kiwaan, F.S. Mohamed, A.A. El-Bindary, N.A. El-Ghamaz, H.R. Abo-Yassin, M.A. El-Bindary, Synthesis, identification and application of metal organic framework for removal of industrial cationic dyes, J. Mol. Liq., 342 (2021) 117435, doi: 10.1016/j.molliq.2021.117435.
[39] N. Hassan, A. Shahat, A. El-Didamony, M. El-Desouky, A.A. El-Bindary, Equilibrium, kinetic and thermodynamic studies of adsorption of cationic dyes from aqueous solution using ZIF-8, Moroccan J. Chem., 8 (2020) 2627–2637.
[40] N. Hassan, A. Shahat, A. El-Didamony, M.G. El-Desouky, A.A. El-Bindary, Mesoporous iron oxide nano spheres for capturing organic dyes from water sources, J. Mol. Struct., 1217 (2020) 128361, doi: 10.1016/j.molstruc.2020.128361.
[41] M.G. El-Desouky, A. Shahat, A.A. El-Bindary, M.A. El-Bindary, Description, kinetic and equilibrium studies of the adsorption of carbon dioxide in mesoporous iron oxide nanospheres, Biointerface Res. Appl. Chem., 12 (2022) 1022–1038.
[42] P.J. Beldon, L. Fábián, R.S. Stein, A. Thirumurugan, A.K. Cheetham, T. Friščić, Rapid room-temperature synthesis of zeolitic imidazolate frameworks by using mechanochemistry, Angew. Chem. Int. Ed., 122 (2010) 9834–9837.
[43] G.A.A. Al-Hazmi, M.A. El-Bindary, M.G. El-Desouky, A.A. El-Bindary, Efficient adsorptive removal of industrial dye from aqueous solution by synthesized zeolitic imidazolate

framework-8 loaded date seed activated carbon and statistical physics modeling, Desal. Water Treat., 7 (2022) 1151–1171.
[44] M.G. El-Desouky, N. Hassan, A. Shahat, A. El-Didamony, A.A. El-Bindary, Synthesis and characterization of porous magnetite nanosphere iron oxide as a novel adsorbent of anionic dyes removal from aqueous solution, Biointerface Res. Appl. Chem., 11 (2021) 13377–13401.
[45] M.I. El-Khaiary, G.F. Malash, Common data analysis errors in batch adsorption studies, Hydrometallurgy, 105 (2011) 314–320.
[46] G.S. dos Reis, R.M.A.P. Lima, S.H. Larsson, C.M. Subramaniyam, V.M. Dinh, M. Thyrel, H.P. de Oliveira, Flexible supercapacitors of biomass-based activated carbon-polypyrrole on eggshell membranes, J. Environ. Chem. Eng., 9 (2021) 106155, doi: 10.1016/j.jece.2021.106155.
[47] M.G. El-Desouky, M.A. El-Bindary, A.A. El-Bindary, Effective adsorptive removal of anionic dyes from aqueous solution, Vietnam J. Chem., 59 (2021) 341–361.
[48] M.A. El-Bindary, M.G. El-Desouky, A.A. El-Bindary, Adsorption of industrial dye from aqueous solutions onto thermally treated green adsorbent: a complete batch system evaluation, J. Mol. Liq., 346 (2021) 117082, doi: 10.1016/j.molliq.2021.117082.
[49] A.S. Al-Wasidi, I.I.S. AlZahrani, H.I. Thawibaraka, A.M. Naglah, M.G. El-Desouky, M.A. El-Bindary, Adsorption studies of carbon dioxide and anionic dye on green adsorbent, J. Mol. Struct., 1250 (2021) 131736, doi: 10.1016/j.molstruc.2021.131736.
[50] K.Y. Foo, B.H. Hameed, Insights into the modeling of adsorption isotherm systems, Chem. Eng. J., 156 (2010) 2–10.
[51] H.N. Tran, S.-J. You, A. Hosseini-Bandegharaei, H.-P. Chao, Mistakes and inconsistencies regarding adsorption of contaminants from aqueous solutions: a critical review, Water Res., 120 (2017) 88–116.
[52] M. Özacar, İ.A. Şengil, Adsorption of reactive dyes on calcined alunite from aqueous solutions, J. Hazard. Mater., 98 (2003) 211–224.
[53] A.S. Al-Wasidi, I.I.S. AlZahrani, A.M. Naglah, M.G. El-Desouky, M.A. Khalil, A.A. El-Bindary, M.A. El-Bindary, Effective removal of methylene blue from aqueous solution using metal-organic framework; modelling analysis, statistical physics treatment and DFT calculations, ChemistrySelect, 6 (2021) 11431–11447.
[54] K. Tan, B. Hameed, Insight into the adsorption kinetics models for the removal of contaminants from aqueous solutions, J. Taiwan Inst. Chem. Eng., 74 (2017) 25–48.
[55] E.C. Lima, A.A. Gomes, H.N. Tran, Comparison of the nonlinear and linear forms of the van't Hoff equation for calculation of adsorption thermodynamic parameters ($\Delta S°$ and $\Delta H°$), J. Mol. Liq., 311 (2020) 113315, doi: 10.1016/j.molliq.2020.113315.
[56] S. Al-Asheh, M. Bagheri, A. Aidan, Membrane bioreactor for wastewater treatment: a review, Case Stud. Chem. Environ. Eng., 4 (2021) 100109, doi: 10.1016/j.cscee.2021.100109.
[57] M.G. El-Desouky, A.A. El-Bindary, M.A. El-Bindary, Low-temperature adsorption study of carbon dioxide on porous magnetite nanospheres iron oxide, Biointerface Res. Appl. Chem., 12 (2021) 6252–6268.
[58] C. Djilani, R. Zaghdoudi, F. Djazi, B. Bouchekima, A. Lallam, A. Modarressi, M. Rogalski, Adsorption of dyes on activated carbon prepared from apricot stones and commercial activated carbon, J. Taiwan Inst. Chem. Eng., 53 (2015) 112–121.
[59] H. Freundlich, W. Heller, The adsorption of cis-and trans-azobenzene, J. Am. Chem. Soc., 61 (1939) 2228–2230.
[60] I. Langmuir, The constitution and fundamental properties of solids and liquids. II. Liquids, J. Am. Chem. Soc., 39 (1917) 1848–1906.
[61] I. Langmuir, The adsorption of gases on plane surfaces of glass, mica and platinum, J. Am. Chem. Soc., 40 (1918) 1361–1403.
[62] R. Rezaei, M. Massinaei, A.Z. Moghaddam, Removal of the residual xanthate from flotation plant tailings using modified bentonite, Miner. Eng., 119 (2018) 1–10.
[63] M. Dubinin, Sorbtsiya I Struktura Aktivnykh Uglei 1. Issledovanie Adsorbtsii Organicheskikh Parov, Zhurnal Fizicheskoi Khimii, 21 (1947) 1351–1362.
[64] M.G. El-Desouky, M.A. Khalil, A.A. El-Bindary, M.A. ElBindary, Biological, biochemical and thermochemical techniques for biofuel production: an updated review, Biointerface Res. Appl. Chem., 12 (2022) 3034–3054.
[65] S. Lagergren, About the theory of so-called adsorption of soluble substances, J. Sven. Vetenskapsakad. Handingarl., 24 (1898) 1–39.
[66] Y.-S. Ho, G. McKay, Sorption of dye from aqueous solution by peat, Chem. Eng. J., 70 (1998) 115–124.
[67] J. Zeldowitsch, Über den mechanismus der katalytischen oxydation von CO an MnO_2, Acta Phys. URSS, 1 (1934) 364–449.
[68] M. Fathi, A. Asfaram, A. Farhangi, Removal of Direct Red 23 from aqueous solution using corn stalks: isotherms, kinetics and thermodynamic studies, Spectrochim. Acta, Part A, 135 (2015) 364–372.
[69] C. Prasad, S. Karlapudi, P. Venkateswarlu, I. Bahadur, S. Kumar, Green arbitrated synthesis of Fe_3O_4 magnetic nanoparticles with nanorod structure from pomegranate leaves and Congo red dye degradation studies for water treatment, J. Mol. Liq., 240 (2017) 322–328.
[70] S. Ziane, F. Bessaha, K. Marouf-Khelifa, A. Khelifa, Single and binary adsorption of reactive black 5 and Congo red on modified dolomite: performance and mechanism, J. Mol. Liq., 249 (2018) 1245–1253.
[71] V.S. Munagapati, V. Yarramuthi, Y. Kim, K.M. Lee, D.-S. Kim, Removal of anionic dyes (Reactive Black 5 and Congo red) from aqueous solutions using Banana Peel Powder as an adsorbent, Ecotoxicol. Environ. Saf., 148 (2018) 601–607.
[72] X.-J. Jia, J. Wang, J. Wu, W. Teng, B. Zhao, H. Li, Y. Du, Facile synthesis of MoO_2/$CaSO_4$ composites as highly efficient adsorbents for Congo red and rhodamine B, RSC Adv., 8 (2018) 1621–1631.
[73] H. Chen, S. Wageh, A.A. Al-Ghamdi, H. Wang, J. Yu, C. Jiang, Hierarchical C/NiO-ZnO nanocomposite fibers with enhanced adsorption capacity for Congo red, J. Colloid Interface Sci., 537 (2019) 736–745.
[74] S. Ghanavati Nasab, A. Semnani, A. Teimouri, H. Kahkesh, T. Momeni Isfahani, S. Habibollahi, Removal of Congo red from aqueous solution by hydroxyapatite nanoparticles loaded on zein as an efficient and green adsorbent: response surface methodology and artificial neural network-genetic algorithm, J. Polym. Environ., 26 (2018) 3677–3697.
[75] G. Bayramoglu, M.Y. Arica, Adsorption of Congo red dye by native amine and carboxyl modified biomass of *Funalia trogii*: isotherms, kinetics and thermodynamics mechanisms, Korean J. Chem. Eng., 35 (2018) 1303–1311.
[76] S.-L. Chan, Y.P. Tan, A.H. Abdullah, S.-T. Ong, Equilibrium, kinetic and thermodynamic studies of a new potential biosorbent for the removal of Basic Blue 3 and Congo red dyes: Pineapple (*Ananas comosus*) plant stem, J. Taiwan Inst. Chem. Eng., 61 (2016) 306–315.

Supporting information

S1. Chemicals

Chemicals were utilized exactly as they were supplied, without any further processing. They include zinc nitrate hexahydrate (99%, Tianjin Kemiou Chemical Reagent, China), N,N-dimethylformamide, anhydrous ethanol (99.7%, Sinopharm Chemical Reagent Co., Ltd., China) and Congo red (CR) were purchased Merck KGaA, 64271 Darmstadt, Germany.

S2. Characterization

Fourier-transform infrared spectra (KBr discs, 4,000–400 cm^{-1}) by JASCO-4100 Spectrophotometer (Japan). The structural differences of the as-prepared Ag-MOF were investigated using the X-ray diffraction (XRD) method. The

powder XRD patterns were captured using a Siemens D500 X-ray Diffractometer (Germany) equipped with a Cu Ka source of radiation. UV-Visible spectra from a PerkinElmer AA800 Spectrophotometer Model AAS with a 1.0 cm model system (China). The pH meter utilized was a WTW 720 Model Digital pH Meter (Germany). On ASAP 2020, the surface area was calculated to use the Brunauer–Emmett–Teller (BET) method, and the pore volume of the BET surfaces and the Barrett–Joyner–Halenda (BJH) surface were calculated (Micrometrics, USA). Scanning electron microscopy (JEOL, JSM-7600F, Japan) was used to examine the microstructure of Ag-MOF. The specimen was then deposited onto a copper substrate after being sputter-coated with a homogenous gold layer. Energy-dispersive X-ray spectroscopy was used to analyze the elemental distribution of Ag-MOF on a Leo1430VP Microscope with a 5 kV operating voltage. X-ray photoelectron spectroscopy was measured using K-ALPHA (Thermo Fisher Scientific, USA).